



Observation of the $\Lambda_b^0 \rightarrow \Lambda_c^+ K^+ K^- \pi^-$ decay

LHCb Collaboration



ARTICLE INFO

Article history:

Received 4 December 2020

Received in revised form 18 February 2021

Accepted 18 February 2021

Available online 23 February 2021

Editor: L. Rolandi

ABSTRACT

The $\Lambda_b^0 \rightarrow \Lambda_c^+ K^+ K^- \pi^-$ decay is observed for the first time using a data sample of proton-proton collisions at centre-of-mass energies of $\sqrt{s} = 7$ and 8 TeV collected by the LHCb detector, corresponding to an integrated luminosity of 3fb^{-1} . The ratio of branching fractions between the $\Lambda_b^0 \rightarrow \Lambda_c^+ K^+ K^- \pi^-$ and the $\Lambda_b^0 \rightarrow \Lambda_c^+ D_s^-$ decays is measured to be

$$\frac{\mathcal{B}(\Lambda_b^0 \rightarrow \Lambda_c^+ K^+ K^- \pi^-)}{\mathcal{B}(\Lambda_b^0 \rightarrow \Lambda_c^+ D_s^-)} = (9.26 \pm 0.29 \pm 0.46 \pm 0.26) \times 10^{-2},$$

where the first uncertainty is statistical, the second systematic and the third is due to the knowledge of the $D_s^- \rightarrow K^+ K^- \pi^-$ branching fraction. No structure on the invariant mass distribution of the $\Lambda_c^+ K^+$ system is found, consistent with no open-charm pentaquark signature.

© 2021 The Author(s). Published by Elsevier B.V. This is an open access article under the CC BY license (<http://creativecommons.org/licenses/by/4.0/>). Funded by SCOAP³.

1. Introduction

Over the last two decades, a wealth of information has been accumulated on the decays of hadrons containing b quarks [1]. Measurements of their decay rates and properties have been used to test the Cabibbo-Kobayashi-Maskawa mechanism [2,3] describing weak interactions within the Standard Model, and to examine various theoretical approaches, such as the heavy quark effective theory [4] and the factorization hypothesis [5–8]. Although many b -hadron decays have been observed with their branching fractions measured, a large number of them remains either unobserved or poorly measured, most notably decays of Λ_b^0 , Ξ_b and Ω_b^- baryons. In the last years, the LHCb experiment has observed many new Λ_b^0 decays to final states such as $\Lambda_c^+ \pi^- \pi^+ \pi^-$ [9], $\Lambda_c^+ \pi^- p\bar{p}$ [10], $\Lambda_c^+ D_s^-$ [11], $\chi_{c1} pK^-$, $\chi_{c2} pK^-$ [12], $\psi(2S) pK^-$ and $J/\psi \pi^+ \pi^- pK^-$ [13].¹

In this Letter, the first observation of the $\Lambda_b^0 \rightarrow \Lambda_c^+ K^+ K^- \pi^-$ decay (referred to hereafter as signal channel) is reported, along with a measurement of its branching fraction relative to that of the $\Lambda_b^0 \rightarrow \Lambda_c^+ D_s^-$ decay (normalisation channel). The analysis uses a data sample of proton-proton (pp) collisions at centre-of-mass energies of $\sqrt{s} = 7$ and 8 TeV collected by the LHCb experiment, corresponding to an integrated luminosity of 3fb^{-1} . The observation of the $\Lambda_b^0 \rightarrow \Lambda_c^+ K^+ K^- \pi^-$ decay provides a laboratory to search for open-charm pentaquarks with valence quark content

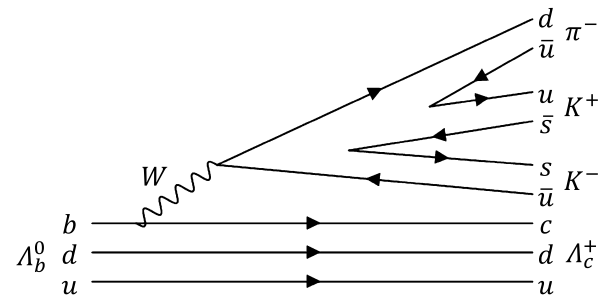


Fig. 1. Feynman diagram of the leading contribution to the $\Lambda_b^0 \rightarrow \Lambda_c^+ K^+ K^- \pi^-$ signal decay.

$c\bar{s}uud$ that could decay strongly to the $\Lambda_c^+ K^+$ final state. These states are a natural extension of the three narrow pentaquark candidates with quark content $c\bar{c}uud$ observed in $\Lambda_b^0 \rightarrow J/\psi pK^-$ decays [14], with the \bar{c} quark replaced by an \bar{s} quark. The recent discovery of a $D^+ K^-$ structure in $B^- \rightarrow D^- D^+ K^-$ decays [15,16], consistent with open-charm tetraquarks, also motivates the search for open-charm pentaquarks.

Fig. 1 shows the leading diagram contributing to the signal decay. Contributions to the companion $K^+ K^- \pi^-$ system could be through intermediate a_1^- mesons, such as the $a_1(1260)^-$ state, which is found to dominate in $\bar{B} \rightarrow D^{(*)} K^{*0} K^-$ decays [17]. Decays of $\Sigma_c^0 \rightarrow \Lambda_c^+ \pi^-$ or even $\Xi_c^0 \rightarrow \Lambda_c^+ K^-$ could also contribute to the signal.

¹ The charge-conjugate process is implied throughout this Letter.

2. Detector and simulation

The LHCb detector [18,19] is a single-arm forward spectrometer covering the pseudorapidity range $2 < \eta < 5$, designed for the study of particles containing b or c quarks. The detector includes a high-precision tracking system consisting of a silicon-strip vertex (VELO) detector surrounding the pp interaction region, a large-area silicon-strip detector located upstream of a dipole magnet with a bending power of about 4Tm, and three stations of silicon-strip detectors and straw drift tubes placed downstream of the magnet. The tracking system provides a measurement of the momentum, p , of charged particles with a relative uncertainty that varies from 0.5% at low momentum to 1.0% at 200 GeV/c. The minimum distance of a track to a primary pp collision vertex (PV), the impact parameter (IP), is measured with a resolution of $(15 + 29/p_T)\mu\text{m}$, where p_T is the component of the momentum transverse to the beam, in GeV/c. Different types of charged hadrons are distinguished using information from two ring-imaging Cherenkov detectors. Photons, electrons and hadrons are identified by a calorimeter system consisting of scintillating-pad and preshower detectors, an electromagnetic and a hadronic calorimeter (HCAL). Muons are identified by a system composed of alternating layers of iron and multiwire proportional chambers.

The online event selection is performed by a trigger based on signal information only. The trigger consists of a hardware stage, based on information from the calorimeter system, followed by a software stage, which applies a full event reconstruction [20]. At the hardware trigger stage, referred to as L0 trigger in the following, the $\Lambda_b^0 \rightarrow \Lambda_c^+ K^+ K^- \pi^-$ and $\Lambda_b^0 \rightarrow \Lambda_c^+ D_s^-$ candidates are required to include a hadron having high transverse energy deposited in the calorimeters. The transverse energy threshold is 3.5 GeV. The software trigger, also named high-level trigger (HLT), requires a two-, three- or four-track vertex with a significant displacement from any PV. At least one charged particle must have a large transverse momentum and be inconsistent with originating from any PV. A multivariate algorithm [21] is used for the identification of displaced vertices consistent with the decay of a b -hadron.

Simulation is used to model the effects of the detector acceptance and the selection requirements, to validate the fit models and to evaluate efficiencies. In the simulation, pp collisions are generated using PYTHIA 8 [22] with a specific LHCb configuration [23]. Decays of unstable particles are described by EVTGEN [24], in which final-state radiation is generated using PHOTOS [25]. The interaction of the generated particles with the detector, and its response, are implemented using the GEANT4 toolkit [26] as described in Ref. [27].

3. Event selection

Candidate Λ_c^+ and D_s^- hadrons are reconstructed through their decays to the $pK^-\pi^+$ and $K^+K^-\pi^-$ final states, respectively. The offline candidate selection is performed by applying a loose preselection, followed by a multivariate analysis (MVA) to further suppress combinatorial background originating from random combinations. To reduce systematic uncertainties on the ratio of efficiencies between the signal and the normalisation channels, the selection criteria of Λ_c^+ candidates are identical between the two channels.

A good-quality track with $p_T > 100\text{ MeV}/c$ and $p > 1\text{ GeV}/c$ is required for each final-state particle. Protons and antiprotons are required to have a momentum greater than $10\text{ GeV}/c$ to improve their identification. All final-state particles are also required to be inconsistent with originating from any PV by requiring a large χ_{IP}^2 , where χ_{IP}^2 is defined as the difference in the χ^2 of a given PV fit with and without the track under consideration. Each Λ_c^+ baryon candidate is required to have at least one decay product

with $p_T > 500\text{ MeV}/c$ and $p > 5\text{ GeV}/c$, a good-quality vertex (*i.e.* small χ_{vtx}^2), and invariant mass within $\pm 15\text{ MeV}/c^2$ of the known Λ_c^+ mass [1]. For the Λ_c^+ candidates, the sum of transverse momenta of their decay products must exceed $1.8\text{ GeV}/c$. The selection criteria for D_s^- candidates are similar to those of Λ_c^+ candidates. The $K^+K^-\pi^-$ invariant mass is required to be within $\pm 35\text{ MeV}/c^2$ from the known D_s^- meson mass.

The signal channel is reconstructed by combining Λ_c^+ , K^+ , K^- and π^- candidates, while the normalisation channel is reconstructed by combining a Λ_c^+ with a D_s^- candidate. The combinations above form Λ_b^0 candidates, which are required to have a small χ_{vtx}^2 and χ_{IP}^2 , and a decay time with respect to its associated PV greater than 0.2 ps. The associated PV is the one that gives the smallest χ_{IP}^2 , where the χ_{IP}^2 denotes the IP significance of candidate's trajectory returned by the kinematical fit. The angle between the Λ_b^0 momentum and the vector pointing from the associated PV to the Λ_b^0 decay vertex, θ_p , is required to be smaller than 11 mrad. The Λ_b^0 candidate is also required to have at least one final-state particle with $p_T > 1.7\text{ GeV}/c$, and its decay vertex significantly displaced from any PV. The latter is achieved by requiring the significance of the flight distance between the Λ_b^0 decay vertex and any PV to be larger than 4. Final-state tracks of signal and normalisation candidates must pass stringent particle-identification requirements based on the information from RICH detectors, calorimeter system and muon stations. To reject tracks that share the same segment in the VELO detector, any two tracks with the same charge used to form the Λ_b^0 candidate are required to have an opening angle larger than 0.5 mrad. A kinematic fit [28] of the decay chain constrains the Λ_b^0 candidate to originate from the associated PV and the Λ_c^+ candidate invariant mass to its known value [1].

The Λ_b^0 candidate could originate from $\bar{B}^0 \rightarrow D^+ K^+ K^- \pi^-$ or $\bar{B}_s^0 \rightarrow D_s^+ K^+ K^- \pi^-$ decays, where a pion or kaon in $D^+ \rightarrow K^+\pi^-\pi^+$ or $D_s^+(D^+) \rightarrow K^+K^-\pi^+$ decays is misidentified as a proton. These background contributions are vetoed if the invariant masses of the Λ_c^+ and Λ_b^0 candidates, evaluated by replacing the proton by either the pion or kaon mass hypothesis, are within $\pm 15\text{ MeV}/c^2$ of the known $D^+(D_s^+)$ mass and $\pm 25\text{ MeV}/c^2$ of the known $\bar{B}^0(\bar{B}_s^0)$ mass [1]. These vetoes are applied to both the signal and the normalisation channels. For the signal decay, additional vetoes are applied if the invariant mass of the $K^+\pi^-$ or $K^+K^-\pi^-$ companion tracks falls within $\pm 30\text{ MeV}/c^2$ of the \bar{D}^0 or D_s^- known mass, respectively [1].

Reconstructed candidates are further required to pass an MVA output threshold based upon a multilayer perceptron (MLP) filter [29], designed to reject the combinatorial background. The MLP classifier is trained using a signal sample of simulated $\Lambda_b^0 \rightarrow \Lambda_c^+ K^+ K^- \pi^-$ decays tuned on data to reproduce correctly the Λ_b^0 production kinematics based on the p_T and y distributions and a background sample taken from the upper sideband of the Λ_b^0 invariant mass spectrum in the range of $5.75 - 7\text{ GeV}/c^2$. A four-body phase-space simulation is used for the signal sample to keep the MLP efficiency as uniform as possible, as including intermediate resonances in the simulation could potentially lead to small MLP efficiencies for less represented phase-space regions. The lower sideband is not used to avoid potential background contributions from partially reconstructed decays. The MLP input includes the following variables: p_T sum of the Λ_c^+ decay products, minimal χ_{IP}^2 among the Λ_c^+ decay products, minimal p_T and minimal χ_{IP}^2 among the kaons originating directly from the Λ_b^0 decay, p_T and χ_{IP}^2 of the π^- from the Λ_b^0 decay, p_T sum of all π and K originating directly from the Λ_b^0 decay, χ_{vtx}^2 of the Λ_c^+ candidate, χ^2 of the flight distance between the Λ_b^0 decay vertex and the associated PV, $\cos\theta_p$, χ^2 probability of the Λ_b^0 candidate ver-

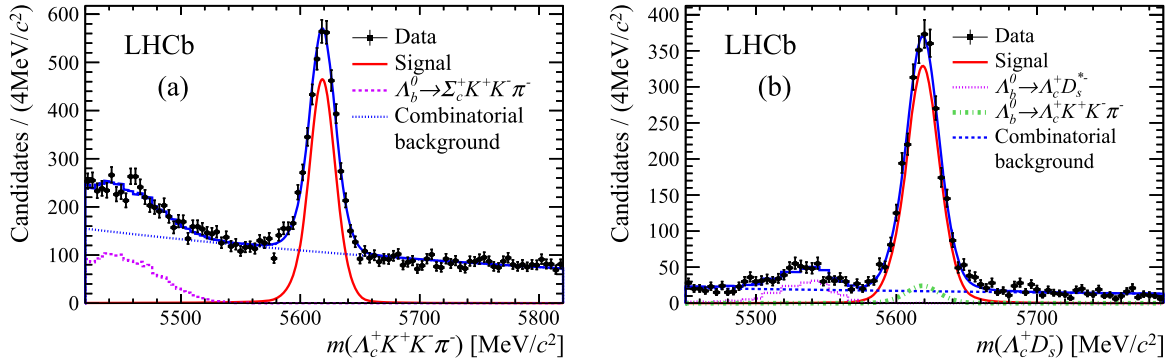


Fig. 2. Invariant mass distribution of (a) $\Lambda_b^0 \rightarrow \Lambda_c^+ K^+ K^- \pi^-$ and (b) $\Lambda_b^0 \rightarrow \Lambda_c^+ D_s^-$ candidates. Fit projections are overlaid as a blue solid line. For (a), the red solid line represents the signal component, the blue dashed line is the background due to random combinations, and the violet dotted line is the contribution from $\Lambda_b^0 \rightarrow \Sigma_c^+ K^+ K^- \pi^-$ decays. For (b), the red solid line is the normalization channel component, the violet dotted line is the $\Lambda_b^0 \rightarrow \Lambda_c^+ D_s^{*-}$ background, the green dashed-dotted line is the contribution from $\Lambda_b^0 \rightarrow \Lambda_c^+ K^+ K^- \pi^-$ decays, and the blue dashed line represents combinatorial background.

tex fit, and the difference of longitudinal position between the Λ_c^+ and the Λ_b^0 decay vertices.

The MLP response obtained from the training is also applied to the normalisation channel sample. The optimal thresholds on the MLP response are obtained for the signal and normalisation channels separately by maximising a figure-of-merit, defined as $S/\sqrt{S+B}$, where S and B are the expected signal and background yields for Λ_b^0 candidates within a $\pm 2.5\sigma$ mass window around the known Λ_b^0 mass [1], where σ is the mass resolution corresponding to about $12 \text{ MeV}/c^2$. Both S and B are determined by multiplying the initial yields of signal and background with the corresponding MLP selection efficiencies estimated from simulation and sideband data, respectively. The initial signal and background yields are obtained from a preliminary fit to the preselected data sample before the MLP requirement applied, where the signal Λ_b^0 peak is already seen in the $\Lambda_c^+ K^+ K^- \pi^-$ invariant mass distribution. The optimal point corresponds to a signal efficiency of 90% and a background rejection of 85%. About 0.6% events in the signal channel contain multiple candidates, only one candidate is retained by a random selection.

4. Signal yields and search for intermediate states

The yields in both the signal and normalisation channels are determined from an unbinned extended maximum-likelihood fit to the corresponding invariant mass spectra of the $\Lambda_c^+ K^+ K^- \pi^-$ system. The signal component is modelled by a sum of two Crystal Ball functions [30] with a common mean of the Gaussian cores, with tail parameters fixed to the values obtained from simulation. For both the signal and normalisation channels, the combinatorial background is described by an exponential function, whose parameters are varied freely and allowed to be different between the signal and normalisation channels. For the signal channel, a significant contribution from $\Lambda_b^0 \rightarrow \Sigma_c^+ [\rightarrow \Lambda_c^+ \pi^0] K^+ K^- \pi^-$ decays is present in the lower invariant mass region, which has the same final state as the π^0 is not reconstructed. The shape of this background is obtained from a simulation of $\Lambda_b^0 \rightarrow \Sigma_c(2455)^+ K^+ K^- \pi^-$ decays. For the normalisation channel, the $\Lambda_b^0 \rightarrow \Lambda_c^+ D_s^{*-}$ decay may be reconstructed as $\Lambda_b^0 \rightarrow \Lambda_c^+ D_s^-$ due to photon emission in the D_s^{*-} decay. The shape of this background is obtained from simulated $\Lambda_b^0 \rightarrow \Lambda_c^+ D_s^{*-}$ decays. The signal decay can also contribute to the normalisation channel forming a background under the D_s^- mass peak. This background contribution is estimated from the D_s^- sidebands of the normalisation data sample, where the width of the sideband is chosen to be the same as that of the D_s^- mass window used in the normalisation channel selection. The

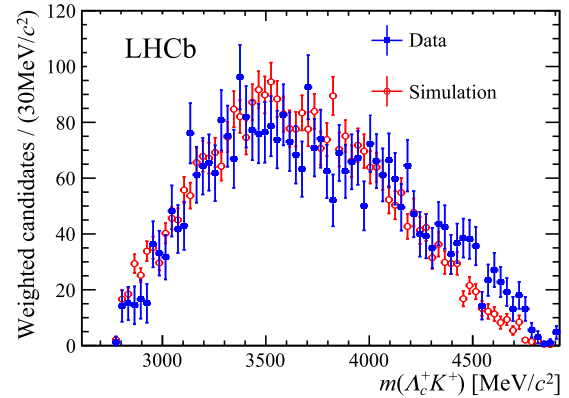


Fig. 3. Invariant mass distributions of $\Lambda_c^+ K^+$ candidates in the $\Lambda_b^0 \rightarrow \Lambda_c^+ K^+ K^- \pi^-$ signal channel for the simulation (red line) and the background-subtracted data (blue points with error bars).

invariant mass distributions for the signal and normalisation channels are shown in Fig. 2 with the fit projects overlaid. The signal yields are obtained to be $N(\Lambda_b^0 \rightarrow \Lambda_c^+ K^+ K^- \pi^-) = 3400 \pm 80$ and $N(\Lambda_b^0 \rightarrow \Lambda_c^+ D_s^- [K^+ K^- \pi^-]) = 2550 \pm 60$, respectively, where the uncertainties are statistical only.

An open-charm pentaquark state could be revealed as a structure in the invariant mass distribution of the $\Lambda_c^+ K^+$ system, shown in Fig. 3 for data and simulation. The data distribution is background subtracted through the *sPlot* weighting technique [31], using the $\Lambda_c^+ K^+ K^- \pi^-$ invariant mass as discriminating variable. No structure is observed. A full amplitude analysis is needed to estimate the limit of the pentaquark contribution, which is beyond the scope of this Letter.

Instead, a rich structure of known hadron contributions is visible in the background-subtracted invariant mass distributions of the $\Lambda_c^+ \pi^-$, $K^+ \pi^-$ and $K^+ K^- \pi^-$ systems, shown in Fig. 4. The $\Sigma_c(2455)^0$ and $\Sigma_c(2520)^0$ resonances are visible in the $\Lambda_c^+ \pi^-$ distribution. A large $K^*(892)^0$ resonance is observed in the $K^+ \pi^-$ projection. In the $K^+ K^- \pi^-$ system, a broad peaking structure at about $1.5 \text{ GeV}/c^2$ is also observed. A similar structure is also seen in $\bar{B} \rightarrow D^{(*)} K^{*0} K^-$ decays by the Belle experiment [17], and is explained as the tail contribution of the $a_1(1260)^-$ resonance.

5. Branching fraction ratio and efficiencies

The ratio of the branching fractions of the $\Lambda_b^0 \rightarrow \Lambda_c^+ K^+ K^- \pi^-$ decay including resonance contributions with respect to the normalisation channel is determined by

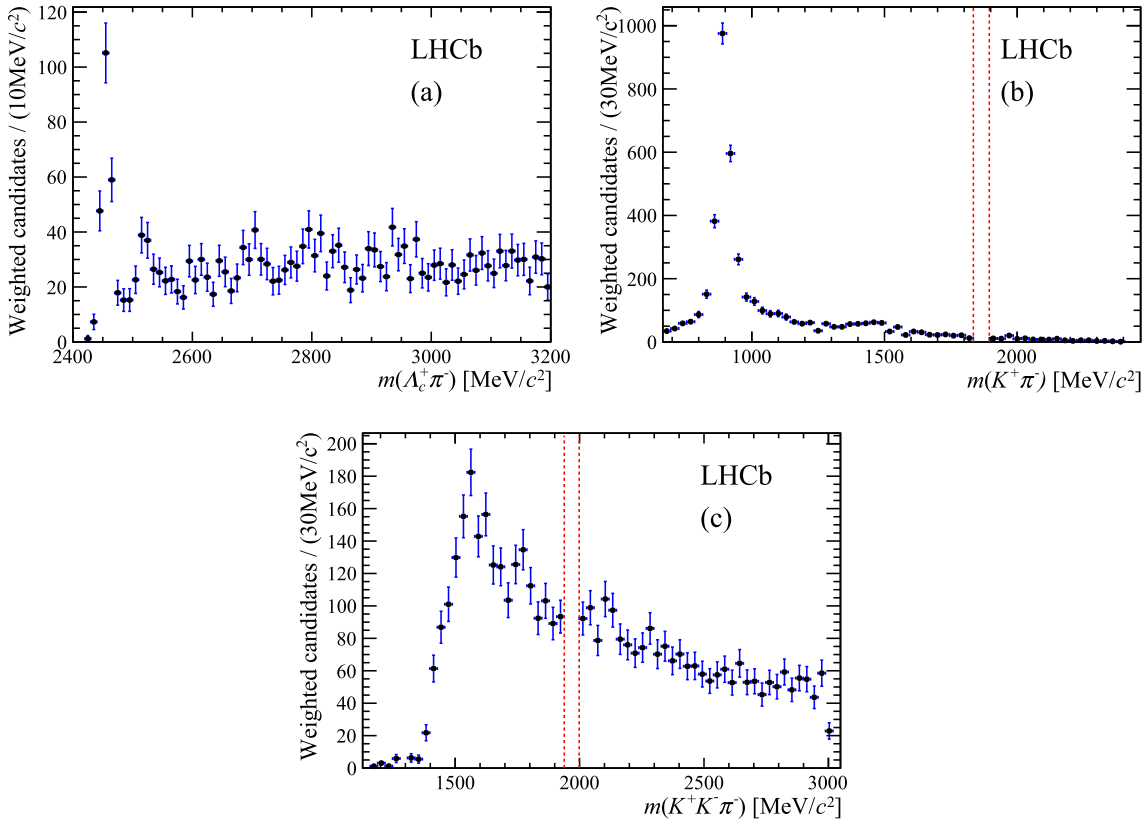


Fig. 4. Invariant mass distributions of (a) the $\Lambda_c^+ \pi^-$, (b) $K^+ \pi^-$, and (c) $K^+ K^- \pi^-$ systems in the $\Lambda_b^0 \rightarrow \Lambda_c^+ K^+ K^- \pi^-$ signal channel, for the background-subtracted data. The red dashed vertical lines indicate the veto mass intervals for D^0 mesons in the $K^+ \pi^-$ distribution, and D_s^- in the $K^+ K^- \pi^-$ distribution.

$$\frac{\mathcal{B}(\Lambda_b^0 \rightarrow \Lambda_c^+ K^+ K^- \pi^-)}{\mathcal{B}(\Lambda_b^0 \rightarrow \Lambda_c^+ D_s^-)} = \frac{N(\Lambda_b^0 \rightarrow \Lambda_c^+ K^+ K^- \pi^-)}{N(\Lambda_b^0 \rightarrow \Lambda_c^+ D_s^- [K^+ K^- \pi^-])} \times \frac{\epsilon_{\text{tot}}(\Lambda_b^0 \rightarrow \Lambda_c^+ D_s^- [K^+ K^- \pi^-])}{\epsilon_{\text{tot}}(\Lambda_b^0 \rightarrow \Lambda_c^+ K^+ K^- \pi^-)}, \quad (1)$$

where \mathcal{B} stands for the branching fraction of the corresponding decay. The signal and normalisation yields are reported in Sec. 4. The total efficiencies ϵ_{tot} of the signal and the normalisation channels are determined by the product

$$\epsilon_{\text{tot}} = \epsilon_{\text{acc}} \times \epsilon_{\text{sel}} \times \epsilon_{\text{L0}} \times \epsilon_{\text{HLT}} \times \epsilon_{\text{PID}}, \quad (2)$$

where ϵ_{acc} accounts for the LHCb geometrical acceptance, ϵ_{sel} is the efficiency of reconstructing and selecting a candidate within the acceptance, ϵ_{L0} is the L0 trigger efficiency for the selected candidates, ϵ_{HLT} is the HLT efficiency for the selected candidates passing the L0 trigger requirement, and ϵ_{PID} is the particle-identification (PID) efficiency for the selected candidates that survive all trigger requirements. All efficiencies except for ϵ_{L0} and ϵ_{PID} are determined from simulation, and the (p_T , y) distributions of the simulated Λ_b^0 baryons are weighted to match that of data, where y is the rapidity of the candidate. The weights are obtained using the normalisation channel and applied to the signal decay.

To take into account the resonance contributions to the signal decay channel, the simulation uses a mixture of three decay modes: $\Lambda_b^0 \rightarrow \Lambda_c^+ a_1(1260)^-(\rightarrow K^{*0} K^-)$, $\Lambda_c^+ K^{*0} K^-$ and non-resonant four-body phase space. The fractions are determined by fitting the two-dimensional data distribution of $K^+ \pi^-$ and $K^+ K^- \pi^-$ invariant masses.

The L0 efficiency of each hadron is computed using samples of well identified pions and kaons from $D^0 \rightarrow K^- \pi^+$ decays and protons from $\Lambda \rightarrow p \pi^-$ decays [32]. The efficiency is calculated in bins of transverse energy for the particles incident on the HCAL surface, separately for its inner and outer regions. The PID efficiency is determined by the calibration samples of $D^{*+} \rightarrow D^0 (\rightarrow K^- \pi^+) \pi^+$ and $\Lambda \rightarrow p \pi^-$ decays and is evaluated as a function of track momentum, track pseudorapidity and event multiplicity, where the latter is represented by the number of the reconstructed tracks in the event.

The ratio between the total efficiencies for the signal and normalisation channels in Eq. (1), is determined to be 0.78 ± 0.02 , where the uncertainty accounts only for the size of the simulation sample. The value differs from unity primarily due to different selection efficiencies on the MVA responses for the signal and normalisation channels.

External inputs are used for the branching fractions $\mathcal{B}(D_s^- \rightarrow K^+ K^- \pi^-) = (5.39 \pm 0.15) \times 10^{-2}$ [1] and $\mathcal{B}(\Lambda_b^0 \rightarrow \Lambda_c^+ D_s^-) = (1.10 \pm 0.10) \times 10^{-2}$ [11]. In the latter case, while the value is measured by the LHCb collaboration [11], its uncertainty is dominated by the branching fraction of $\bar{B}^0 \rightarrow D^+ D_s^-$ decays, and is essentially uncorrelated with the present measurement.

6. Systematic uncertainties

All systematic uncertainties on the measurement of the ratio of branching fractions are listed in Table 1. The total uncertainty is determined from the sum of all contributions in quadrature. The dominant uncertainty is related to the resonance structure that is not perfectly modelled by the simulation.

Uncertainties due to the fit model are considered. For the background due to random combinations of final-state particles in both

Table 1

Summary of systematic uncertainties on the ratio of branching fractions.

Source	Uncertainty (%)
Combinatorial background	0.9
Shape of $\Lambda_b^0 \rightarrow \Sigma_c^+ K^+ K^- \pi^-$ contribution	0.3
$\Lambda_b^0 \rightarrow \Lambda_c^+ K^+ K^- \pi^-$ background in normalisation channel	0.8
Signal fit model	0.5
Simulation sample size	2.5
PID efficiency	0.4
Trigger efficiency	0.1
(p_T, y) weight	0.8
Track multiplicity weight	0.8
Λ_c^+ Dalitz structure	1.4
Mixture fraction in simulation	0.2
Resonance structure	3.6
Multiple candidates	0.3
MVA selection	0.5
Total	4.9

the signal and normalisation channels, the exponential function is replaced by a second-order polynomial function. From the comparison to the default result, the relative uncertainty on the ratio of branching fractions is 0.9%. In the signal channel, the uncertainty due to the $\Lambda_b^0 \rightarrow \Sigma_c^+ K^+ K^- \pi^-$ background contribution is assessed by performing the fit with a widened mass region, resulting in a relative uncertainty of 0.3%. For the normalisation channel, changing the yield of the $\Lambda_b^0 \rightarrow \Lambda_c^+ K^+ K^- \pi^-$ contribution within its uncertainty results in a relative 0.8% variation.

The systematic uncertainty due to the model for both signal and normalisation channels, is studied by changing to a single Hypatia function [33], where the mean and width parameters are left free while all other parameters are taken from simulation. This results in a relative uncertainty of 0.5%.

The uncertainties on the ratio of efficiencies are evaluated. The uncertainty due to the finite simulation sample size is evaluated from the expected efficiency variation in bins of p_T and y of the Λ_b^0 candidate as

$$\sigma_\epsilon = \sqrt{\sum_i \epsilon_i (1 - \epsilon_i) N_i w_i} / \sum_i N_i w_i, \quad (3)$$

for each bin i , where N_i is the number of generated events, w_i is a correction weight, and ϵ_i is the candidate efficiency. The normalisation of the weights is chosen such that the denominator is equal to total number of generated events without the weighting. The relative uncertainty is found to be 2.5%.

Pseudoexperiments are used to evaluate the systematic effects due to uncertainties on the weights or efficiencies in different bins. For a given source, many pseudoexperiments are generated, in which each produces a new set of weights or efficiencies according to the central values and uncertainties following Gaussian distributions. The efficiency ratio between the signal and normalisation channels is recomputed. The resulting efficiency ratios from many pseudoexperiments of this source produce a Gaussian distribution centering at the baseline value. The standard deviation of the Gaussian distribution is taken as absolute uncertainty on the efficiency ratio for the given source. The procedure is applied to obtain the systematic uncertainty related to the PID and trigger efficiencies and to (p_T, y) and track multiplicity weighting.

The tracking efficiency returned by the simulation is calibrated using a data-driven method [34]. The uncertainty on the calibration sample size is propagated to the efficiency ratio using pseudoexperiments, resulting in a systematic uncertainty of 0.8%. Because the final states for signal and normalisation modes are identical,

possible data-simulation differences in hadron interactions with the detector material are assumed to be negligible.

The agreement between data and simulation for the $\Lambda_c^+ \rightarrow p K^- \pi^+$ channel is tested by comparing the Dalitz structure. The signal simulation sample is weighted in the $m(pK^-)$ versus $m(K^- \pi^+)$ plane to match the distribution of the background-subtracted data. The uncertainty related to the limited sample size used for obtaining these weights is 1.1%, obtained from pseudo-experiments. The uncertainty related to the choice of binning is 0.8%, determined by using an alternative binning. A total of 1.4% is assigned as systematic uncertainty.

The contributions of the Λ_b^0 decays through the mixture of the three decay modes are considered when generating the simulated events of the signal channel, and their fractions are obtained by fitting the two-dimensional distribution of the $K^+ K^- \pi^-$ and $K^+ \pi^-$ systems in the background-subtracted signal data. The fractions are changed according to the statistical uncertainty of the fit result, yielding 0.2% of relative uncertainty.

The simulation does not fully model the resonance structure, e.g. the contribution of Σ_c^0 resonances, which is clearly seen in the $\Lambda_c^+ \pi^-$ invariant mass distribution, as illustrated in Fig. 4. By weighting the simulation to match the $m(\Lambda_c^+ \pi^-)$ distribution in the data, a 1.3% variation of the ratio of branching fractions is found and assigned as systematic uncertainty. Besides, differences between background-subtracted data and simulated signal events are also observed in the invariant mass distributions of the $\Lambda_c^+ K^+ K^-$ and $K^+ K^-$ systems. To account for this discrepancy, the simulated sample is weighted according to the $\Lambda_c^+ K^+ K^-$ or $K^+ K^-$ mass distribution of background-subtracted data, and the ratio of branching fractions is reevaluated. The two procedures return changes of 2.6% and 2.0%, respectively. The three values are added in quadrature to account for the uncertainty due to resonance structure.

Simulation does not account well for multiple candidates, which is found to be about 0.6% of the data sample in the signal channel. Half of this fraction is assigned as systematic uncertainty due to the random choice to retain only one candidate.

The MVA selection criteria are optimized separately for the signal and normalisation channels. As an alternative choice, the MVA selection of the normalisation channel is fixed to be the same as that of the signal channel to test the robustness of the MVA selection. The relative variation of the branching fraction ratio is 0.5%, which is assigned as systematic uncertainty.

7. Results and summary

The first observation of the $\Lambda_b^0 \rightarrow \Lambda_c^+ K^+ K^- \pi^-$ decay is presented, and the branching fraction is determined using the $\Lambda_b^0 \rightarrow \Lambda_c^+ D_s^-$ decay as a normalisation channel. The relative branching fraction is measured to be

$$\frac{\mathcal{B}(\Lambda_b^0 \rightarrow \Lambda_c^+ K^+ K^- \pi^-)}{\mathcal{B}(\Lambda_b^0 \rightarrow \Lambda_c^+ D_s^-)} = (9.26 \pm 0.29 \pm 0.46 \pm 0.26) \times 10^{-2},$$

where the first uncertainty is statistical, the second systematic, and the third is due to the knowledge of the $D_s^- \rightarrow K^+ K^- \pi^-$ branching fraction [1]. Using this ratio, the $\Lambda_b^0 \rightarrow \Lambda_c^+ K^+ K^- \pi^-$ branching fraction is determined to be

$$\mathcal{B}(\Lambda_b^0 \rightarrow \Lambda_c^+ K^+ K^- \pi^-) = (1.02 \pm 0.03 \pm 0.05 \pm 0.10) \times 10^{-3},$$

where the third term includes the uncertainty on the branching fraction of the $\Lambda_b^0 \rightarrow \Lambda_c^+ D_s^-$ decay [1]. The invariant mass distribution of the $\Lambda_c^+ K^+$ system is inspected for possible structure due to open-charm pentaquarks, and no contribution is observed.

Declaration of competing interest

The authors declare that they have no known competing financial interests or personal relationships that could have appeared to influence the work reported in this paper.

Acknowledgements

We express our gratitude to our colleagues in the CERN accelerator departments for the excellent performance of the LHC. We thank the technical and administrative staff at the LHCb institutes. We acknowledge support from CERN and from the national agencies: CAPES, CNPq, FAPERJ and FINEP (Brazil); MOST and NSFC (China); CNRS/IN2P3 (France); BMBF, DFG and MPG (Germany); INFN (Italy); NWO (Netherlands); MNiSW and NCN (Poland); MEN/IFA (Romania); MSHE (Russia); MICINN (Spain); SNSF and SER (Switzerland); NASU (Ukraine); STFC (United Kingdom); DOE NP and NSF (USA). We acknowledge the computing resources that are provided by CERN, IN2P3 (France), KIT and DESY (Germany), INFN (Italy), SURF (Netherlands), PIC (Spain), GridPP (United Kingdom), RRCKI and Yandex LLC (Russia), CSCS (Switzerland), IFIN-HH (Romania), CBPF (Brazil), PL-GRID (Poland) and OSC (USA). We are indebted to the communities behind the multiple open-source software packages on which we depend. Individual groups or members have received support from AvH Foundation (Germany); EPLANET, Marie Skłodowska-Curie Actions and ERC (European Union); A*MIDEX, ANR, Labex P2IO and OCEVU, and Région Auvergne-Rhône-Alpes (France); Key Research Program of Frontier Sciences of CAS, CAS PIPI, Thousand Talents Program, and Sci. & Tech. Program of Guangzhou (China); RFBR, RSF and Yandex LLC (Russia); GVA, XuntaGal and GENCAT (Spain); The Royal Society and the Leverhulme Trust (United Kingdom).

Appendix A. Supplementary material

Supplementary material related to this article can be found online at <https://doi.org/10.1016/j.physletb.2021.136172>.

References

- [1] Particle Data Group, P.A. Zyla, et al., Review of particle physics, to be published in *Prog. Theor. Exp. Phys.* 6 (2020) 083C01.
- [2] N. Cabibbo, Unitary symmetry and leptonic decays, *Phys. Rev. Lett.* 10 (1963) 531.
- [3] M. Kobayashi, T. Maskawa, CP-violation in the renormalizable theory of weak interaction, *Prog. Theor. Phys.* 49 (1973) 652.
- [4] E. Eichten, B. Hill, An effective field theory for the calculation of matrix elements involving heavy quarks, *Phys. Lett. B* 234 (1990) 511.
- [5] D. Fakirov, B. Stech, F and D decays, *Nucl. Phys. B* 133 (1978) 315.
- [6] N. Cabibbo, L. Maiani, Two-body decays of charmed mesons, *Phys. Lett. B* 73 (1978) 418, Erratum: *Phys. Lett. B* 76 (1978) 663.
- [7] T. Mannel, W. Roberts, Z. Ryzak, Factorization hypothesis and the non-leptonic decays of heavy hadrons, *Phys. Lett. B* 259 (1991) 359.
- [8] M. Beneke, G. Buchalla, M. Neubert, C.T. Sachrajda, QCD factorization for exclusive non-leptonic b-meson decays: general arguments and the case of heavy-light final states, *Nucl. Phys. B* 591 (2000) 313.
- [9] LHCb collaboration, R. Aaij, et al., Measurements of the branching fractions for $B_{(s)}^0 \rightarrow D_{(s)}\pi\pi\pi$ and $\Lambda_b^0 \rightarrow \Lambda_c^+\pi\pi\pi$, *Phys. Rev. D* 84 (2011) 092001, Erratum: *Phys. Rev. D* 85 (2012) 039904, arXiv:1109.6831.
- [10] LHCb collaboration, R. Aaij, et al., Observation of the decay $\Lambda_b^0 \rightarrow \Lambda_c^+ p\bar{p}\pi^-$, *Phys. Lett. B* 784 (2018) 101, arXiv:1804.09617.
- [11] LHCb collaboration, R. Aaij, et al., Study of beauty hadron decays into pairs of charm hadrons, *Phys. Rev. Lett.* 112 (2014) 202001, arXiv:1403.3606.
- [12] LHCb collaboration, R. Aaij, et al., Observation of the decays $\Lambda_b^0 \rightarrow \chi_{c1}pK^-$ and $\Lambda_b^0 \rightarrow \chi_{c2}pK^-$, *Phys. Rev. Lett.* 119 (2017) 062001, arXiv:1704.07900.
- [13] LHCb collaboration, R. Aaij, et al., Observation of $\Lambda_b^0 \rightarrow \psi(2S)pK^-$ and $\Lambda_b^0 \rightarrow J/\psi\pi^+pK^-$ decays and a measurement of the Λ_b^0 baryon mass, *J. High Energy Phys.* 05 (2016) 132, arXiv:1603.06961.
- [14] LHCb collaboration, R. Aaij, et al., Observation of a narrow pentaquark state, $P_c(4312)^+$, and of two-peak structure of the $P_c(4450)^+$, *Phys. Rev. Lett.* 122 (2019) 222001, arXiv:1904.03947.
- [15] LHCb collaboration, R. Aaij, et al., Model-independent study of structure in $B^+p \rightarrow D^+D^-K^+$ decays, *Phys. Rev. Lett.* 125 (2020) 242001, arXiv:2009.00025.
- [16] LHCb collaboration, R. Aaij, et al., Amplitude analysis of the $B^+ \rightarrow D^+D^-K^+$ decay, *Phys. Rev. D* 102 (2020) 112003, arXiv:2009.00026.
- [17] Belle collaboration, A. Drutskoy, et al., Observation of $B \rightarrow D^{(*)}K^-K^{0(*)}$ decays, *Phys. Lett. B* 542 (2002) 171, arXiv:hep-ex/0207041.
- [18] LHCb collaboration, A.A. Alves Jr, et al., The LHCb detector at the LHC, *J. Instrum.* 3 (2008) S08005.
- [19] LHCb collaboration, R. Aaij, et al., LHCb detector performance, *Int. J. Mod. Phys. A* 30 (2015) 1530022, arXiv:1412.6352.
- [20] R. Aaij, et al., The LHCb trigger and its performance in 2011, *J. Instrum.* 8 (2013) P04022, arXiv:1211.3055.
- [21] V.V. Gligorov, M. Williams, Efficient, reliable and fast high-level triggering using a bonsai boosted decision tree, *J. Instrum.* 8 (2013) P02013, arXiv:1210.6861.
- [22] T. Sjöstrand, S. Mrenna, P. Skands, A brief introduction to PYTHIA 8.1, *Comput. Phys. Commun.* 178 (2008) 852, arXiv:0710.3820.
- [23] I. Belyaev, et al., Handling of the generation of primary events in Gauss, the LHCb simulation framework, *J. Phys. Conf. Ser.* 331 (2011) 032047.
- [24] D.J. Lange, The EvtGen particle decay simulation package, *Nucl. Instrum. Methods A* 462 (2001) 152.
- [25] P. Golonka, Z. Was, PHOTOS Monte Carlo: a precision tool for QED corrections in Z and W decays, *Eur. Phys. J. C* 45 (2006) 97, arXiv:hep-ph/0506026.
- [26] Geant4 collaboration, J. Allison, et al., Geant4 developments and applications, *IEEE Trans. Nucl. Sci.* 53 (2006) 270;
- [27] Geant4 collaboration, S. Agostinelli, et al., A simulation toolkit, *Nucl. Instrum. Methods A* 506 (2003) 250.
- [28] M. Clemencic, et al., The LHCb simulation application, Gauss: design, evolution and experience, *J. Phys. Conf. Ser.* 331 (2011) 032023.
- [29] W.D. Hulsbergen, Decay chain fitting with a Kalman filter, *Nucl. Instrum. Methods A* 552 (2005) 566, arXiv:physics/0503191.
- [30] A. Hoecker, et al., TMVA 4 – toolkit for multivariate data analysis with ROOT. Users guide, arXiv:physics/0703039.
- [31] T. Skwarnicki, A study of the radiative cascade transitions between the Upsilon-prime and Upsilon resonances, PhD thesis Institute of Nuclear Physics, Krakow, 1986, DESY-F31-86-02.
- [32] M. Pivk, F.R. Le Diberder, sPlot: a statistical tool to unfold data distributions, *Nucl. Instrum. Methods A* 555 (2005) 356, arXiv:physics/0402083.
- [33] A. Martin Sanchez, P. Robbe, M.-H. Schune, Performances of the LHCb L0 Calorimeter Trigger, LHCb-PUB-2011-026, CERN-LHCb-PUB-2011-026, 2012.
- [34] D. Martínez Santos, F. Duprétius, Mass distributions marginalized over per-event errors, *Nucl. Instrum. Methods A* 764 (2014) 150, arXiv:1312.5000.
- [35] LHCb collaboration, R. Aaij, et al., Measurement of the track reconstruction efficiency at LHCb, *J. Instrum.* 10 (2015) P02007, arXiv:1408.1251.

LHCb Collaboration

R. Aaij ³¹, C. Abellán Beteta ⁴⁹, T. Ackernley ⁵⁹, B. Adeua ⁴⁵, M. Adinolfi ⁵³, H. Afsharnia ⁹, C.A. Aidala ⁸⁴, S. Aiola ²⁵, Z. Ajaltouni ⁹, S. Akar ⁶⁴, J. Albrecht ¹⁴, F. Alessio ⁴⁷, M. Alexander ⁵⁸, A. Alfonso Albero ⁴⁴, Z. Aliouche ⁶¹, G. Alkhazov ³⁷, P. Alvarez Cartelle ⁴⁷, S. Amato ², Y. Amhis ¹¹, L. An ²¹, L. Anderlini ²¹, A. Andreianov ³⁷, M. Andreotti ²⁰, F. Archilli ¹⁶, A. Artamonov ⁴³, M. Artuso ⁶⁷, K. Arzymatov ⁴¹, E. Aslanides ¹⁰, M. Atzeni ⁴⁹, B. Audurier ¹¹, S. Bachmann ¹⁶, M. Bachmayer ⁴⁸, J.J. Back ⁵⁵, S. Baker ⁶⁰, P. Baladron Rodriguez ⁴⁵, V. Balagura ¹¹, W. Baldini ²⁰, J. Baptista Leite ¹, R.J. Barlow ⁶¹, S. Barsuk ¹¹, W. Barter ⁶⁰, M. Bartolini ^{23,i}, F. Baryshnikov ⁸⁰, J.M. Basels ¹³, G. Bassi ²⁸, B. Batsukh ⁶⁷, A. Battig ¹⁴, A. Bay ⁴⁸, M. Becker ¹⁴, F. Bedeschi ²⁸, I. Bediaga ¹, A. Beiter ⁶⁷, V. Belavin ⁴¹, S. Belin ²⁶, V. Bellee ⁴⁸,

- K. Belous ⁴³, I. Belov ³⁹, I. Belyaev ³⁸, G. Bencivenni ²², E. Ben-Haim ¹², A. Berezhnoy ³⁹, R. Bernet ⁴⁹, D. Berninghoff ¹⁶, H.C. Bernstein ⁶⁷, C. Bertella ⁴⁷, E. Bertholet ¹², A. Bertolin ²⁷, C. Betancourt ⁴⁹, F. Betti ^{19,e}, M.O. Bettler ⁵⁴, Ia. Bezshyiko ⁴⁹, S. Bhasin ⁵³, J. Bhom ³³, L. Bian ⁷², M.S. Bieker ¹⁴, S. Bifani ⁵², P. Billoir ¹², M. Birch ⁶⁰, F.C.R. Bishop ⁵⁴, A. Bizzeti ^{21,s}, M. Bjørn ⁶², M.P. Blago ⁴⁷, T. Blake ⁵⁵, F. Blanc ⁴⁸, S. Blusk ⁶⁷, D. Bobulska ⁵⁸, J.A. Boelhauve ¹⁴, O. Boente Garcia ⁴⁵, T. Boettcher ⁶³, A. Boldyrev ⁸¹, A. Bondar ^{42,v}, N. Bondar ³⁷, S. Borghi ⁶¹, M. Borisjak ⁴¹, M. Borsato ¹⁶, J.T. Borsuk ³³, S.A. Bouchiba ⁴⁸, T.J.V. Bowcock ⁵⁹, A. Boyer ⁴⁷, C. Bozzi ²⁰, M.J. Bradley ⁶⁰, S. Braun ⁶⁵, A. Brea Rodriguez ⁴⁵, M. Brodski ⁴⁷, J. Brodzicka ³³, A. Brossa Gonzalo ⁵⁵, D. Brundu ²⁶, A. Buonaura ⁴⁹, C. Burr ⁴⁷, A. Bursche ²⁶, A. Butkevich ⁴⁰, J.S. Butter ³¹, J. Buytaert ⁴⁷, W. Byczynski ⁴⁷, S. Cadeddu ²⁶, H. Cai ⁷², R. Calabrese ^{20,g}, L. Calefice ¹⁴, L. Calero Diaz ²², S. Cali ²², R. Calladine ⁵², M. Calvi ^{24,j}, M. Calvo Gomez ⁸³, P. Camargo Magalhaes ⁵³, A. Camboni ⁴⁴, P. Campana ²², D.H. Campora Perez ⁴⁷, A.F. Campoverde Quezada ⁵, S. Capelli ^{24,j}, L. Capriotti ^{19,e}, A. Carbone ^{19,e}, G. Carboni ²⁹, R. Cardinale ^{23,i}, A. Cardini ²⁶, I. Carli ⁶, P. Carniti ^{24,j}, L. Carus ¹³, K. Carvalho Akiba ³¹, A. Casais Vidal ⁴⁵, G. Casse ⁵⁹, M. Cattaneo ⁴⁷, G. Cavallero ⁴⁷, S. Celani ⁴⁸, J. Cerasoli ¹⁰, A.J. Chadwick ⁵⁹, M.G. Chapman ⁵³, M. Charles ¹², Ph. Charpentier ⁴⁷, G. Chatzikonstantinidis ⁵², C.A. Chavez Barajas ⁵⁹, M. Chefdeville ⁸, C. Chen ³, S. Chen ²⁶, A. Chernov ³³, S.-G. Chitic ⁴⁷, V. Chobanova ⁴⁵, S. Cholak ⁴⁸, M. Chrzaszcz ³³, A. Chubykin ³⁷, V. Chulikov ³⁷, P. Ciambrone ²², M.F. Cicala ⁵⁵, X. Cid Vidal ⁴⁵, G. Ciezarek ⁴⁷, P.E.L. Clarke ⁵⁷, M. Clemencic ⁴⁷, H.V. Cliff ⁵⁴, J. Closier ⁴⁷, J.L. Cobbledick ⁶¹, V. Coco ⁴⁷, J.A.B. Coelho ¹¹, J. Cogan ¹⁰, E. Cogneras ⁹, L. Cojocariu ³⁶, P. Collins ⁴⁷, T. Colombo ⁴⁷, L. Congedo ¹⁸, A. Contu ²⁶, N. Cooke ⁵², G. Coombs ⁵⁸, G. Corti ⁴⁷, C.M. Costa Sobral ⁵⁵, B. Couturier ⁴⁷, D.C. Craik ⁶³, J. Crkovská ⁶⁶, M. Cruz Torres ¹, R. Currie ⁵⁷, C.L. Da Silva ⁶⁶, E. Dall'Occo ¹⁴, J. Dalseno ⁴⁵, C. D'Ambrosio ⁴⁷, A. Danilina ³⁸, P. d'Argent ⁴⁷, A. Davis ⁶¹, O. De Aguiar Francisco ⁶¹, K. De Bruyn ⁷⁷, S. De Capua ⁶¹, M. De Cian ⁴⁸, J.M. De Miranda ¹, L. De Paula ², M. De Serio ^{18,d}, D. De Simone ⁴⁹, P. De Simone ²², J.A. de Vries ⁷⁸, C.T. Dean ⁶⁶, W. Dean ⁸⁴, D. Decamp ⁸, L. Del Buono ¹², B. Delaney ⁵⁴, H.-P. Dembinski ¹⁴, A. Dendek ³⁴, V. Denysenko ⁴⁹, D. Derkach ⁸¹, O. Deschamps ⁹, F. Desse ¹¹, F. Dettori ^{26,f}, B. Dey ⁷², P. Di Nezza ²², S. Didenko ⁸⁰, L. Dieste Maronas ⁴⁵, H. Dijkstra ⁴⁷, V. Dobishuk ⁵¹, A.M. Donohoe ¹⁷, F. Dordei ²⁶, A.C. dos Reis ¹, L. Douglas ⁵⁸, A. Dovbnya ⁵⁰, A.G. Downes ⁸, K. Dreimanis ⁵⁹, M.W. Dudek ³³, L. Dufour ⁴⁷, V. Duk ⁷⁶, P. Durante ⁴⁷, J.M. Durham ⁶⁶, D. Dutta ⁶¹, M. Dziewiecki ¹⁶, A. Dziurda ³³, A. Dzyuba ³⁷, S. Easo ⁵⁶, U. Egede ⁶⁸, V. Egorychev ³⁸, S. Eidelman ^{42,v}, S. Eisenhardt ⁵⁷, S. Ek-In ⁴⁸, L. Eklund ⁵⁸, S. Ely ⁶⁷, A. Ene ³⁶, E. Epple ⁶⁶, S. Escher ¹³, J. Eschle ⁴⁹, S. Esen ³¹, T. Evans ⁴⁷, A. Falabella ¹⁹, J. Fan ³, Y. Fan ⁵, B. Fang ⁷², N. Farley ⁵², S. Farry ⁵⁹, D. Fazzini ^{24,j}, P. Fedin ³⁸, M. Féo ⁴⁷, P. Fernandez Declara ⁴⁷, A. Fernandez Prieto ⁴⁵, J.M. Fernandez-tenllado Arribas ⁴⁴, F. Ferrari ^{19,e}, L. Ferreira Lopes ⁴⁸, F. Ferreira Rodrigues ², S. Ferreres Sole ³¹, M. Ferrillo ⁴⁹, M. Ferro-Luzzi ⁴⁷, S. Filippov ⁴⁰, R.A. Fini ¹⁸, M. Fiorini ^{20,g}, M. Firlej ³⁴, K.M. Fischer ⁶², C. Fitzpatrick ⁶¹, T. Fiutowski ³⁴, F. Fleuret ^{11,b}, M. Fontana ⁴⁷, F. Fontanelli ^{23,i}, R. Forty ⁴⁷, V. Franco Lima ⁵⁹, M. Franco Sevilla ⁶⁵, M. Frank ⁴⁷, E. Franzoso ²⁰, G. Frau ¹⁶, C. Frei ⁴⁷, D.A. Friday ⁵⁸, J. Fu ²⁵, Q. Fuehring ¹⁴, W. Funk ⁴⁷, E. Gabriel ³¹, T. Gaintseva ⁴¹, A. Gallas Torreira ⁴⁵, D. Galli ^{19,e}, S. Gambetta ⁵⁷, Y. Gan ³, M. Gandelman ², P. Gandini ²⁵, Y. Gao ⁴, M. Garau ²⁶, L.M. Garcia Martin ⁵⁵, P. Garcia Moreno ⁴⁴, J. García Pardiñas ⁴⁹, B. Garcia Plana ⁴⁵, F.A. Garcia Rosales ¹¹, L. Garrido ⁴⁴, D. Gascon ⁴⁴, C. Gaspar ⁴⁷, R.E. Geertsema ³¹, D. Gerick ¹⁶, L.L. Gerken ¹⁴, E. Gersabeck ⁶¹, M. Gersabeck ⁶¹, T. Gershon ⁵⁵, D. Gerstel ¹⁰, Ph. Ghez ⁸, V. Gibson ⁵⁴, M. Giovannetti ^{22,k}, A. Gioventù ⁴⁵, P. Gironella Gironell ⁴⁴, L. Giubega ³⁶, C. Giugliano ^{20,g}, K. Gisdov ⁵⁷, E.L. Gkougkousis ⁴⁷, V.V. Gligorov ¹², C. Göbel ⁶⁹, E. Golobardes ⁸³, D. Golubkov ³⁸, A. Golutvin ^{60,80}, A. Gomes ^{1,a}, S. Gomez Fernandez ⁴⁴, F. Goncalves Abrantes ⁶⁹, M. Goncerz ³³, G. Gong ³, P. Gorbounov ³⁸, I.V. Gorelov ³⁹, C. Gotti ^{24,j}, E. Govorkova ³¹, J.P. Grabowski ¹⁶, R. Graciani Diaz ⁴⁴, T. Grammatico ¹², L.A. Granado Cardoso ⁴⁷, E. Graugés ⁴⁴, E. Graverini ⁴⁸, G. Graziani ²¹, A. Grecu ³⁶, L.M. Greeven ³¹, P. Griffith ²⁰, L. Grillo ⁶¹, S. Gromov ⁸⁰, L. Gruber ⁴⁷, B.R. Gruberg Cazon ⁶², C. Gu ³, M. Guarise ²⁰, P.A. Günther ¹⁶, E. Gushchin ⁴⁰, A. Guth ¹³, Y. Guz ^{43,47}, T. Gys ⁴⁷, T. Hadavizadeh ⁶⁸, G. Haefeli ⁴⁸, C. Haen ⁴⁷, J. Haimberger ⁴⁷, S.C. Haines ⁵⁴, T. Halewood-leagases ⁵⁹, P.M. Hamilton ⁶⁵, Q. Han ⁷, X. Han ¹⁶, T.H. Hancock ⁶², S. Hansmann-Menzemer ¹⁶, N. Harnew ⁶², T. Harrison ⁵⁹, C. Hasse ⁴⁷, M. Hatch ⁴⁷, J. He ⁵, M. Hecker ⁶⁰, K. Heijhoff ³¹, K. Heinicke ¹⁴, A.M. Hennequin ⁴⁷, K. Hennessy ⁵⁹, L. Henry ^{25,46}, J. Heuel ¹³, A. Hicheur ², D. Hill ⁶², M. Hilton ⁶¹, S.E. Hollitt ¹⁴, P.H. Hopchev ⁴⁸, J. Hu ¹⁶, J. Hu ⁷¹, W. Hu ⁷, W. Huang ⁵, X. Huang ⁷², W. Hulsbergen ³¹, R.J. Hunter ⁵⁵, M. Hushchyn ⁸¹, D. Hutchcroft ⁵⁹, D. Hynds ³¹, P. Ibis ¹⁴, M. Idzik ³⁴, D. Ilin ³⁷, P. Ilten ⁶⁴, A. Inglessi ³⁷, A. Ishteev ⁸⁰,

- K. Ivshin ³⁷, R. Jacobsson ⁴⁷, S. Jakobsen ⁴⁷, E. Jans ³¹, B.K. Jashal ⁴⁶, A. Jawahery ⁶⁵, V. Jevtic ¹⁴, M. Jezabek ³³, F. Jiang ³, M. John ⁶², D. Johnson ⁴⁷, C.R. Jones ⁵⁴, T.P. Jones ⁵⁵, B. Jost ⁴⁷, N. Jurik ⁴⁷, S. Kandybei ⁵⁰, Y. Kang ³, M. Karacson ⁴⁷, M. Karpov ⁸¹, N. Kazeev ⁸¹, F. Keizer ^{54,47}, M. Kenzie ⁵⁵, T. Ketel ³², B. Khanji ⁴⁷, A. Kharisova ⁸², S. Kholodenko ⁴³, K.E. Kim ⁶⁷, T. Kirn ¹³, V.S. Kirsebom ⁴⁸, O. Kitouni ⁶³, S. Klaver ³¹, K. Klimaszewski ³⁵, S. Kolliiev ⁵¹, A. Kondybayeva ⁸⁰, A. Konoplyannikov ³⁸, P. Kopciewicz ³⁴, R. Kopecna ¹⁶, P. Koppenburg ³¹, M. Korolev ³⁹, I. Kostiuk ^{31,51}, O. Kot ⁵¹, S. Kotriakhova ^{37,30}, P. Kravchenko ³⁷, L. Kravchuk ⁴⁰, R.D. Krawczyk ⁴⁷, M. Kreps ⁵⁵, F. Kress ⁶⁰, S. Kretzschmar ¹³, P. Krokovny ^{42,v}, W. Krupa ³⁴, W. Krzemien ³⁵, W. Kucewicz ^{33,l}, M. Kucharczyk ³³, V. Kudryavtsev ^{42,v}, H.S. Kuindersma ³¹, G.J. Kunde ⁶⁶, T. Kvaratskheliya ³⁸, D. Lacarrere ⁴⁷, G. Lafferty ⁶¹, A. Lai ²⁶, A. Lampis ²⁶, D. Lancierini ⁴⁹, J.J. Lane ⁶¹, R. Lane ⁵³, G. Lanfranchi ²², C. Langenbruch ¹³, J. Langer ¹⁴, O. Lantwin ^{49,80}, T. Latham ⁵⁵, F. Lazzari ^{28,t}, R. Le Gac ¹⁰, S.H. Lee ⁸⁴, R. Lefèvre ⁹, A. Leflat ³⁹, S. Legotin ⁸⁰, O. Leroy ¹⁰, T. Lesiak ³³, B. Leverington ¹⁶, H. Li ⁷¹, L. Li ⁶², P. Li ¹⁶, X. Li ⁶⁶, Y. Li ⁶, Z. Li ⁶, X. Liang ⁶⁷, T. Lin ⁶⁰, R. Lindner ⁴⁷, V. Lisovskyi ¹⁴, R. Litvinov ²⁶, G. Liu ⁷¹, H. Liu ⁵, S. Liu ⁶, X. Liu ³, A. Loi ²⁶, J. Lomba Castro ⁴⁵, I. Longstaff ⁵⁸, J.H. Lopes ², G. Loustau ⁴⁹, G.H. Lovell ⁵⁴, Y. Lu ⁶, D. Lucchesi ^{27,m}, S. Luchuk ⁴⁰, M. Lucio Martinez ³¹, V. Lukashenko ³¹, Y. Luo ³, A. Lupato ⁶¹, E. Luppi ^{20,g}, O. Lupton ⁵⁵, A. Lusiani ^{28,r}, X. Lyu ⁵, L. Ma ⁶, S. Maccolini ^{19,e}, F. Machefert ¹¹, F. Maciuc ³⁶, V. Macko ⁴⁸, P. Mackowiak ¹⁴, S. Maddrell-Mander ⁵³, O. Madejczyk ³⁴, L.R. Madhan Mohan ⁵³, O. Maev ³⁷, A. Maevskiy ⁸¹, D. Maisuzenko ³⁷, M.W. Majewski ³⁴, J.J. Malczewski ³³, S. Malde ⁶², B. Malecki ⁴⁷, A. Malinin ⁷⁹, T. Maltsev ^{42,v}, H. Malygina ¹⁶, G. Manca ^{26,f}, G. Mancinelli ¹⁰, R. Manera Escalero ⁴⁴, D. Manuzzi ^{19,e}, D. Marangotto ^{25,o}, J. Maratas ^{9,u}, J.F. Marchand ⁸, U. Marconi ¹⁹, S. Mariani ^{21,47,h}, C. Marin Benito ¹¹, M. Marinangeli ⁴⁸, P. Marino ⁴⁸, J. Marks ¹⁶, P.J. Marshall ⁵⁹, G. Martellotti ³⁰, L. Martinazzoli ^{47,j}, M. Martinelli ^{24,j}, D. Martinez Santos ⁴⁵, F. Martinez Vidal ⁴⁶, A. Massafferri ¹, M. Materok ¹³, R. Matev ⁴⁷, A. Mathad ⁴⁹, Z. Mathe ⁴⁷, V. Matiunin ³⁸, C. Matteuzzi ²⁴, K.R. Mattioli ⁸⁴, A. Mauri ³¹, E. Maurice ^{11,b}, J. Mauricio ⁴⁴, M. Mazurek ³⁵, M. McCann ⁶⁰, L. McConnell ¹⁷, T.H. Mcgrath ⁶¹, A. McNab ⁶¹, R. McNulty ¹⁷, J.V. Mead ⁵⁹, B. Meadows ⁶⁴, C. Meaux ¹⁰, G. Meier ¹⁴, N. Meinert ⁷⁵, D. Melnychuk ³⁵, S. Meloni ^{24,j}, M. Merk ^{31,78}, A. Merli ²⁵, L. Meyer Garcia ², M. Mikhasenko ⁴⁷, D.A. Milanes ⁷³, E. Millard ⁵⁵, M. Milovanovic ⁴⁷, M.-N. Minard ⁸, L. Minzoni ^{20,g}, S.E. Mitchell ⁵⁷, B. Mitreska ⁶¹, D.S. Mitzel ⁴⁷, A. Mödden ¹⁴, R.A. Mohammed ⁶², R.D. Moise ⁶⁰, T. Mombächer ¹⁴, I.A. Monroy ⁷³, S. Monteil ⁹, M. Morandin ²⁷, G. Morello ²², M.J. Morello ^{28,r}, J. Moron ³⁴, A.B. Morris ⁷⁴, A.G. Morris ⁵⁵, R. Mountain ⁶⁷, H. Mu ³, F. Muheim ⁵⁷, M. Mukherjee ⁷, M. Mulder ⁴⁷, D. Müller ⁴⁷, K. Müller ⁴⁹, C.H. Murphy ⁶², D. Murray ⁶¹, P. Muzzetto ²⁶, P. Naik ⁵³, T. Nakada ⁴⁸, R. Nandakumar ⁵⁶, T. Nanut ⁴⁸, I. Nasteva ², M. Needham ⁵⁷, I. Neri ^{20,g}, N. Neri ^{25,o}, S. Neubert ⁷⁴, N. Neufeld ⁴⁷, R. Newcombe ⁶⁰, T.D. Nguyen ⁴⁸, C. Nguyen-Mau ⁴⁸, E.M. Niel ¹¹, S. Nieswand ¹³, N. Nikitin ³⁹, N.S. Nolte ⁴⁷, C. Nunez ⁸⁴, A. Oblakowska-Mucha ³⁴, V. Obraztsov ⁴³, D.P. O'Hanlon ⁵³, R. Oldeman ^{26,f}, M.E. Olivares ⁶⁷, C.J.G. Onderwater ⁷⁷, A. Ossowska ³³, J.M. Otalora Goicochea ², T. Ovsiannikova ³⁸, P. Owen ⁴⁹, A. Oyanguren ^{46,47}, B. Pagare ⁵⁵, P.R. Pais ⁴⁷, T. Pajero ^{28,47,r}, A. Palano ¹⁸, M. Palutan ²², Y. Pan ⁶¹, G. Panshin ⁸², A. Papanestis ⁵⁶, M. Pappagallo ^{18,d}, L.L. Pappalardo ^{20,g}, C. Pappenheimer ⁶⁴, W. Parker ⁶⁵, C. Parkes ⁶¹, C.J. Parkinson ⁴⁵, B. Passalacqua ²⁰, G. Passaleva ²¹, A. Pastore ¹⁸, M. Patel ⁶⁰, C. Patrignani ^{19,e}, C.J. Pawley ⁷⁸, A. Pearce ⁴⁷, A. Pellegrino ³¹, M. Pepe Altarelli ⁴⁷, S. Perazzini ¹⁹, D. Pereima ³⁸, P. Perret ⁹, K. Petridis ⁵³, A. Petrolini ^{23,i}, A. Petrov ⁷⁹, S. Petrucci ⁵⁷, M. Petruzzo ²⁵, T.T.H. Pham ⁶⁷, A. Philippov ⁴¹, L. Pica ²⁸, M. Piccini ⁷⁶, B. Pietrzyk ⁸, G. Pietrzyk ⁴⁸, M. Pili ⁶², D. Pinci ³⁰, J. Pinzino ⁴⁷, F. Pisani ⁴⁷, A. Piucci ¹⁶, P.K. Resmi ¹⁰, V. Placinta ³⁶, S. Playfer ⁵⁷, J. Plews ⁵², M. Plo Casasus ⁴⁵, F. Polci ¹², M. Poli Lener ²², M. Poliakova ⁶⁷, A. Poluektov ¹⁰, N. Polukhina ^{80,c}, I. Polyakov ⁶⁷, E. Polycarpo ², G.J. Pomery ⁵³, S. Ponce ⁴⁷, A. Popov ⁴³, D. Popov ^{5,47}, S. Popov ⁴¹, S. Poslavskii ⁴³, K. Prasant ³³, L. Promberger ⁴⁷, C. Prouve ⁴⁵, V. Pugatch ⁵¹, A. Puig Navarro ⁴⁹, H. Pullen ⁶², G. Punzi ^{28,n}, W. Qian ⁵, J. Qin ⁵, R. Quagliani ¹², B. Quintana ⁸, N.V. Raab ¹⁷, R.I. Rabadan Trejo ¹⁰, B. Rachwal ³⁴, J.H. Rademacker ⁵³, M. Rama ²⁸, M. Ramos Pernas ⁵⁵, M.S. Rangel ², F. Ratnikov ^{41,81}, G. Raven ³², M. Reboud ⁸, F. Redi ⁴⁸, F. Reiss ¹², C. Remon Alepuz ⁴⁶, Z. Ren ³, V. Renaudin ⁶², R. Ribatti ²⁸, S. Ricciardi ⁵⁶, K. Rinnert ⁵⁹, P. Robbe ¹¹, A. Robert ¹², G. Robertson ⁵⁷, A.B. Rodrigues ⁴⁸, E. Rodrigues ⁵⁹, J.A. Rodriguez Lopez ⁷³, A. Rollings ⁶², P. Roloff ⁴⁷, V. Romanovskiy ⁴³, M. Romero Lamas ⁴⁵, A. Romero Vidal ⁴⁵, J.D. Roth ⁸⁴, M. Rotondo ²², M.S. Rudolph ⁶⁷, T. Ruf ⁴⁷, J. Ruiz Vidal ⁴⁶, A. Ryzhikov ⁸¹, J. Ryzka ³⁴, J.J. Saborido Silva ⁴⁵, N. Sagidova ³⁷, N. Sahoo ⁵⁵, B. Saitta ^{26,f}, D. Sanchez Gonzalo ⁴⁴, C. Sanchez Gras ³¹, R. Santacesaria ³⁰, C. Santamarina Rios ⁴⁵, M. Santimaria ²²,

E. Santovetti ^{29,k}, D. Saranin ⁸⁰, G. Sarpis ⁶¹, M. Sarpis ⁷⁴, A. Sarti ³⁰, C. Satriano ^{30,q}, A. Satta ²⁹, M. Saur ⁵,
 D. Savrina ^{38,39}, H. Sazak ⁹, L.G. Scantlebury Smead ⁶², S. Schael ¹³, M. Schellenberg ¹⁴, M. Schiller ⁵⁸,
 H. Schindler ⁴⁷, M. Schmelling ¹⁵, T. Schmelzer ¹⁴, B. Schmidt ⁴⁷, O. Schneider ⁴⁸, A. Schopper ⁴⁷,
 M. Schubiger ³¹, S. Schulte ⁴⁸, M.H. Schune ¹¹, R. Schwemmer ⁴⁷, B. Sciascia ²², A. Sciubba ³⁰, S. Sellam ⁴⁵,
 A. Semennikov ³⁸, M. Senghi Soares ³², A. Sergi ^{52,47}, N. Serra ⁴⁹, J. Serrano ¹⁰, L. Sestini ²⁷, A. Seuthe ¹⁴,
 P. Seyfert ⁴⁷, D.M. Shangase ⁸⁴, M. Shapkin ⁴³, I. Shchemberov ⁸⁰, L. Shchutska ⁴⁸, T. Shears ⁵⁹,
 L. Shekhtman ^{42,v}, Z. Shen ⁴, V. Shevchenko ⁷⁹, E.B. Shields ^{24,j}, E. Shmanin ⁸⁰, J.D. Shupperd ⁶⁷,
 B.G. Siddi ²⁰, R. Silva Coutinho ⁴⁹, G. Simi ²⁷, S. Simone ^{18,d}, I. Skiba ^{20,g}, N. Skidmore ⁷⁴, T. Skwarnicki ⁶⁷,
 M.W. Slater ⁵², J.G. Smeaton ⁵⁴, A. Smetkina ³⁸, E. Smith ¹³, M. Smith ⁶⁰, A. Snoch ³¹, M. Soares ¹⁹,
 L. Soares Lavra ⁹, M.D. Sokoloff ⁶⁴, F.J.P. Soler ⁵⁸, A. Solovev ³⁷, I. Solovyev ³⁷, F.L. Souza De Almeida ²,
 B. Souza De Paula ², B. Spaan ¹⁴, E. Spadaro Norella ^{25,o}, P. Spradlin ⁵⁸, F. Stagni ⁴⁷, M. Stahl ⁶⁴, S. Stahl ⁴⁷,
 P. Steffko ⁴⁸, O. Steinkamp ^{49,80}, S. Stemmle ¹⁶, O. Stenyakin ⁴³, H. Stevens ¹⁴, S. Stone ⁶⁷,
 M.E. Stramaglia ⁴⁸, M. Stratciuc ³⁶, D. Strekalina ⁸⁰, S. Strokov ⁸², F. Suljik ⁶², J. Sun ²⁶, L. Sun ⁷², Y. Sun ⁶⁵,
 P. Svihra ⁶¹, P.N. Swallow ⁵², K. Swientek ³⁴, A. Szabelski ³⁵, T. Szumlak ³⁴, M. Szymanski ⁴⁷, S. Taneja ⁶¹,
 Z. Tang ³, T. Tekampe ¹⁴, F. Teubert ⁴⁷, E. Thomas ⁴⁷, K.A. Thomson ⁵⁹, M.J. Tilley ⁶⁰, V. Tisserand ⁹,
 S. T'Jampens ⁸, M. Tobin ⁶, S. Tolk ⁴⁷, L. Tomassetti ^{20,g}, D. Torres Machado ¹, D.Y. Tou ¹², M. Traill ⁵⁸,
 M.T. Tran ⁴⁸, E. Trifonova ⁸⁰, C. Tripli ⁴⁸, A. Tsaregorodtsev ¹⁰, G. Tuci ^{28,n}, A. Tully ⁴⁸, N. Tuning ³¹,
 A. Ukleja ³⁵, D.J. Unverzagt ¹⁶, E. Ursov ⁸⁰, A. Usachov ³¹, A. Ustyuzhanin ^{41,81}, U. Uwer ¹⁶, A. Vagner ⁸²,
 V. Vagnoni ¹⁹, A. Valassi ⁴⁷, G. Valenti ¹⁹, N. Valls Canudas ⁴⁴, M. van Beuzekom ³¹, M. Van Dijk ⁴⁸,
 H. Van Hecke ⁶⁶, E. van Herwijnen ⁸⁰, C.B. Van Hulse ¹⁷, M. van Veghel ⁷⁷, R. Vazquez Gomez ⁴⁵,
 P. Vazquez Regueiro ⁴⁵, C. Vázquez Sierra ³¹, S. Vecchi ²⁰, J.J. Velthuis ⁵³, M. Veltri ^{21,p},
 A. Venkateswaran ⁶⁷, M. Veronesi ³¹, M. Vesterinen ⁵⁵, D. Vieira ⁶⁴, M. Vieites Diaz ⁴⁸, H. Viemann ⁷⁵,
 X. Vilasis-Cardona ⁸³, E. Vilella Figueras ⁵⁹, P. Vincent ¹², G. Vitali ²⁸, A. Vollhardt ⁴⁹, D. Vom Bruch ¹²,
 A. Vorobyev ³⁷, V. Vorobyev ^{42,v}, N. Voropaev ³⁷, R. Waldi ⁷⁵, J. Walsh ²⁸, C. Wang ¹⁶, J. Wang ³, J. Wang ⁷²,
 J. Wang ⁴, J. Wang ⁶, M. Wang ³, R. Wang ⁵³, Y. Wang ⁷, Z. Wang ⁴⁹, H.M. Wark ⁵⁹, N.K. Watson ⁵²,
 S.G. Weber ¹², D. Websdale ⁶⁰, C. Weisser ⁶³, B.D.C. Westhenry ⁵³, D.J. White ⁶¹, M. Whitehead ⁵³,
 D. Wiedner ¹⁴, G. Wilkinson ⁶², M. Wilkinson ⁶⁷, I. Williams ⁵⁴, M. Williams ^{63,68}, M.R.J. Williams ⁵⁷,
 F.F. Wilson ⁵⁶, W. Wislicki ³⁵, M. Witek ³³, L. Witola ¹⁶, G. Wormser ¹¹, S.A. Wotton ⁵⁴, H. Wu ⁶⁷,
 K. Wyllie ⁴⁷, Z. Xiang ⁵, D. Xiao ⁷, Y. Xie ⁷, H. Xing ⁷¹, A. Xu ⁴, J. Xu ⁵, L. Xu ³, M. Xu ⁷, Q. Xu ⁵, Z. Xu ⁵,
 Z. Xu ^{4,*}, D. Yang ³, Y. Yang ⁵, Z. Yang ³, Z. Yang ⁶⁵, Y. Yao ⁶⁷, L.E. Yeomans ⁵⁹, H. Yin ⁷, J. Yu ⁷⁰, X. Yuan ⁶⁷,
 O. Yushchenko ⁴³, E. Zaffaroni ⁴⁸, K.A. Zarebski ⁵², M. Zavertyaev ^{15,c}, M. Zdybal ³³, O. Zenaiev ⁴⁷,
 M. Zeng ³, D. Zhang ⁷, L. Zhang ³, S. Zhang ⁴, Y. Zhang ⁴⁷, Y. Zhang ⁶², A. Zhelezov ¹⁶, Y. Zheng ⁵, X. Zhou ⁵,
 Y. Zhou ⁵, X. Zhu ³, V. Zhukov ^{13,39}, J.B. Zonneveld ⁵⁷, S. Zucchelli ^{19,e}, D. Zuliani ²⁷, G. Zunica ⁶¹

¹ Centro Brasileiro de Pesquisas Físicas (CBPF), Rio de Janeiro, Brazil² Universidade Federal do Rio de Janeiro (UFRJ), Rio de Janeiro, Brazil³ Center for High Energy Physics, Tsinghua University, Beijing, China⁴ School of Physics State Key Laboratory of Nuclear Physics and Technology, Peking University, Beijing, China⁵ University of Chinese Academy of Sciences, Beijing, China⁶ Institute Of High Energy Physics (IHEP), Beijing, China⁷ Institute of Particle Physics, Central China Normal University, Wuhan, Hubei, China⁸ Univ. Grenoble Alpes, Univ. Savoie Mont Blanc, CNRS, IN2P3-LAPP, Annecy, France⁹ Université Clermont Auvergne, CNRS/IN2P3, LPC, Clermont-Ferrand, France¹⁰ Aix Marseille Univ, CNRS/IN2P3, CPPM, Marseille, France¹¹ Université Paris-Saclay, CNRS/IN2P3, IJCLab, Orsay, France¹² LPNHE, Sorbonne Université, Paris Diderot Sorbonne Paris Cité, CNRS/IN2P3, Paris, France¹³ I. Physikalisches Institut, RWTH Aachen University, Aachen, Germany¹⁴ Fakultät Physik, Technische Universität Dortmund, Dortmund, Germany¹⁵ Max-Planck-Institut für Kernphysik (MPIK), Heidelberg, Germany¹⁶ Physikalisches Institut, Ruprecht-Karls-Universität Heidelberg, Heidelberg, Germany¹⁷ School of Physics, University College Dublin, Dublin, Ireland¹⁸ INFN Sezione di Bari, Bari, Italy¹⁹ INFN Sezione di Bologna, Bologna, Italy²⁰ INFN Sezione di Ferrara, Ferrara, Italy²¹ INFN Sezione di Firenze, Firenze, Italy²² INFN Laboratori Nazionali di Frascati, Frascati, Italy²³ INFN Sezione di Genova, Genova, Italy²⁴ INFN Sezione di Milano-Bicocca, Milano, Italy²⁵ INFN Sezione di Milano, Milano, Italy²⁶ INFN Sezione di Cagliari, Monserrato, Italy²⁷ Università degli Studi di Padova, Università e INFN, Padova, Padova, Italy²⁸ INFN Sezione di Pisa, Pisa, Italy²⁹ INFN Sezione di Roma Tor Vergata, Roma, Italy³⁰ INFN Sezione di Roma La Sapienza, Roma, Italy

- ³¹ Nikhef National Institute for Subatomic Physics, Amsterdam, Netherlands
³² Nikhef National Institute for Subatomic Physics and VU University Amsterdam, Amsterdam, Netherlands
³³ Henryk Niewodniczanski Institute of Nuclear Physics Polish Academy of Sciences, Kraków, Poland
³⁴ AGH - University of Science and Technology, Faculty of Physics and Applied Computer Science, Kraków, Poland
³⁵ National Center for Nuclear Research (NCB), Warsaw, Poland
³⁶ Horia Hulubei National Institute of Physics and Nuclear Engineering, Bucharest-Magurele, Romania
³⁷ Petersburg Nuclear Physics Institute NRC Kurchatov Institute (PNPI NRC KI), Gatchina, Russia
³⁸ Institute of Theoretical and Experimental Physics NRC Kurchatov Institute (ITEP NRC KI), Moscow, Russia
³⁹ Institute of Nuclear Physics, Moscow State University (SINP MSU), Moscow, Russia
⁴⁰ Institute for Nuclear Research of the Russian Academy of Sciences (INR RAS), Moscow, Russia
⁴¹ Yandex School of Data Analysis, Moscow, Russia
⁴² Budker Institute of Nuclear Physics (SB RAS), Novosibirsk, Russia
⁴³ Institute for High Energy Physics NRC Kurchatov Institute (IHEP NRC KI), Protvino, Russia
⁴⁴ ICCUB, Universitat de Barcelona, Barcelona, Spain
⁴⁵ Instituto Galego de Física de Altas Enerxías (IGFAE), Universidade de Santiago de Compostela, Santiago de Compostela, Spain
⁴⁶ Instituto de Física Corpuscular, Centro Mixto Universidad de Valencia - CSIC, Valencia, Spain
⁴⁷ European Organization for Nuclear Research (CERN), Geneva, Switzerland
⁴⁸ Institute of Physics, Ecole Polytechnique Fédérale de Lausanne (EPFL), Lausanne, Switzerland
⁴⁹ Physik-Institut, Universität Zürich, Zürich, Switzerland
⁵⁰ NSC Kharkiv Institute of Physics and Technology (NSC KIPT), Kharkiv, Ukraine
⁵¹ Institute for Nuclear Research of the National Academy of Sciences (KINR), Kyiv, Ukraine
⁵² University of Birmingham, Birmingham, United Kingdom
⁵³ H.H. Wills Physics Laboratory, University of Bristol, Bristol, United Kingdom
⁵⁴ Cavendish Laboratory, University of Cambridge, Cambridge, United Kingdom
⁵⁵ Department of Physics, University of Warwick, Coventry, United Kingdom
⁵⁶ STFC Rutherford Appleton Laboratory, Didcot, United Kingdom
⁵⁷ School of Physics and Astronomy, University of Edinburgh, Edinburgh, United Kingdom
⁵⁸ School of Physics and Astronomy, University of Glasgow, Glasgow, United Kingdom
⁵⁹ Oliver Lodge Laboratory, University of Liverpool, Liverpool, United Kingdom
⁶⁰ Imperial College London, London, United Kingdom
⁶¹ Department of Physics and Astronomy, University of Manchester, Manchester, United Kingdom
⁶² Department of Physics, University of Oxford, Oxford, United Kingdom
⁶³ Massachusetts Institute of Technology, Cambridge, MA, United States
⁶⁴ University of Cincinnati, Cincinnati, OH, United States
⁶⁵ University of Maryland, College Park, MD, United States
⁶⁶ Los Alamos National Laboratory (LANL), Los Alamos, United States
⁶⁷ Syracuse University, Syracuse, NY, United States
⁶⁸ School of Physics and Astronomy, Monash University, Melbourne, Australia, associated to ⁵⁵
⁶⁹ Pontifícia Universidade Católica do Rio de Janeiro (PUC-Rio), Rio de Janeiro, Brazil, associated to ²
⁷⁰ Physics and Micro Electronic College, Hunan University, Changsha City, China, associated to ⁷
⁷¹ Guangdong Provincial Key Laboratory of Nuclear Science, Institute of Quantum Matter, South China Normal University, Guangzhou, China, associated to ³
⁷² School of Physics and Technology, Wuhan University, Wuhan, China, associated to ³
⁷³ Departamento de Física, Universidad Nacional de Colombia, Bogota, Colombia, associated to ¹²
⁷⁴ Universität Bonn - Helmholtz-Institut für Strahlen und Kernphysik, Bonn, Germany, associated to ¹⁶
⁷⁵ Institut für Physik, Universität Rostock, Rostock, Germany, associated to ¹⁶
⁷⁶ INFN Sezione di Perugia, Perugia, Italy, associated to ²⁰
⁷⁷ Van Swinderen Institute, University of Groningen, Groningen, Netherlands, associated to ³¹
⁷⁸ Universiteit Maastricht, Maastricht, Netherlands, associated to ³¹
⁷⁹ National Research Centre Kurchatov Institute, Moscow, Russia, associated to ³⁸
⁸⁰ National University of Science and Technology "MISIS", Moscow, Russia, associated to ³⁸
⁸¹ National Research University Higher School of Economics, Moscow, Russia, associated to ⁴¹
⁸² National Research Tomsk Polytechnic University, Tomsk, Russia, associated to ³⁸
⁸³ DS4DS, La Salle, Universitat Ramon Llull, Barcelona, Spain, associated to ⁴⁴
⁸⁴ University of Michigan, Ann Arbor, United States, associated to ⁶⁷

* Corresponding author.

E-mail address: zexu@cern.ch (Z. Xu).

^a Universidade Federal do Triângulo Mineiro (UFTM), Uberaba-MG, Brazil.

^b Laboratoire Leprince-Ringuet, Palaiseau, France.

^c P.N. Lebedev Physical Institute, Russian Academy of Science (LPI RAS), Moscow, Russia.

^d Università di Bari, Bari, Italy.

^e Università di Bologna, Bologna, Italy.

^f Università di Cagliari, Cagliari, Italy.

^g Università di Ferrara, Ferrara, Italy.

^h Università di Firenze, Firenze, Italy.

ⁱ Università di Genova, Genova, Italy.

^j Università di Milano Bicocca, Milano, Italy.

^k Università di Roma Tor Vergata, Roma, Italy.

^l AGH - University of Science and Technology, Faculty of Computer Science, Electronics and Telecommunications, Kraków, Poland.

^m Università di Padova, Padova, Italy.

ⁿ Università di Pisa, Pisa, Italy.

^o Università degli Studi di Milano, Milano, Italy.

^p Università di Urbino, Urbino, Italy.

^q Università della Basilicata, Potenza, Italy.

^r Scuola Normale Superiore, Pisa, Italy.

^s Università di Modena e Reggio Emilia, Modena, Italy.

^t Università di Siena, Siena, Italy.

^u MSU - Iligan Institute of Technology (MSU-IIT), Iligan, Philippines.

^v Novosibirsk State University, Novosibirsk, Russia.